Magnetic fluctuations and self-energy effects in two-dimensional itinerant systems with a van Hove singularity in the electronic spectrum

P. A. Igoshev,[1,2] V. Yu. Irkhin,[1] and A. A. Katanin[1,2]

[1]*Institute of Metal Physics, Kovalevskaya str. 18, 620990 Ekaterinburg, Russia*

[2]*Max-Planck Institute für Festkörperforschung, DE-70569 Stuttgart, Germany*

(Received 7 December 2010; revised manuscript received 29 April 2011; published 22 June 2011)

We investigate a competition of tendencies toward ferromagnetic and incommensurate order in two-dimensional fermionic systems within functional renormalization-group technique, accounting for the self-energy corrections and using temperature as a scale parameter. We assume that the Fermi surface (FS) is substantially curved and lies in the vicinity of van Hove singularity points. It is shown that the character of magnetic fluctuations is strongly asymmetric with respect to the Fermi level position relative to van Hove singularity (VHS). For the Fermi level above VHS, we find at low temperatures dominant incommensurate magnetic fluctuations, while below the VHS level, we find indications for the ferromagnetic ground state. In agreement with the Mermin-Wagner theorem, at finite temperatures and in small magnetic fields, we obtain small magnetization, which appears to be a power-law function of magnetic field. It is found that the FS curvature is slightly increased by correlation effects, and the renormalized bandwidth decreases at sufficiently low temperatures.

DOI: 10.1103/PhysRevB.83.245118 PACS number(s): 75.30.Kz, 71.10.Fd, 75.10.Lp

I. INTRODUCTION

During the last two decades, the problem of magnetic fluctuations in itinerant-electron compounds attracts substantial interest in connection with the physics of layered systems. In copper-oxide high-temperature superconductors, the importance of magnetic fluctuations is seen from the proximity of an antiferromagnetically ordered region to the region of superconducting state with pronounced incommensurate magnetic fluctuations.[1,2] Another impressive example of peculiar magnetic properties of low-dimensional systems is provided by the family of layered strontium ruthenates, which are pure metallic and incidentally have a very complex magnetic behavior.

Neutron scattering[3] of the one-layer paramagnetic metal Sr_2RuO_4 (which, at low temperatures $T \lesssim 1.5$ K, becomes an unconventional, most likely p-wave, superconductor[4,5]) reveals an incommensurate character of magnetic fluctuation spectrum, with the largest contribution corresponding to the wave vector $\mathbf{Q}_s \sim (2/3)(\pi,\pi)$ and the smaller one with the wave vector $\mathbf{Q}_l \sim \mathbf{Q}_{s/2}$. It was argued[6] that incommensurate short-wave magnetic fluctuations characterized by the wave vector $\mathbf{Q}_s$ are expected to originate from α and β bands [produced by d_{xz} an d_{yz} orbitals and generating quasi-one-dimensional sheets of Fermi surface (FS)], while the long-wave magnetic fluctuations with the wave vector $\mathbf{Q}_l$ originate most likely from the γ band, produced by d_{xy} orbitals and generating quasi-two-dimensional sheets of FS. Moreover, magnetic properties of this compound can be controlled by the substitution effect: being doped by lanthanum, $Sr_{2-y}La_yRuO_4$ exhibits enhancement of magnetic susceptibility. This enhancement is likely related to the position of the Fermi level of the γ band. The fit of the tight-binding spectrum to experimentally determined Fermi surfaces provides an expectation of the onset of the ferromagnetic order at $y = 0.27$, related to the elevation of the Fermi level of the γ band toward a van Hove singularity (VHS). However, despite the VHS at the Fermi level, revealed by angle-resolved photoemission spectroscopy (ARPES),[7] no ferromagnetic order was found for this doping (Ref. 8).

An intriguing behavior of magnetic properties is observed also in $Ca_{2-x}Sr_xRuO_4$ near $x = 0.5$. The band structure calculations[9] and angle-resolved photoemission spectroscopy studies[10] yield that the doping by Ca results in rotation of RuO_6 octahedra and, in turn, in a complex movement of the Fermi level with respect to VHS and reconstruction of the electronic spectrum. The substitution of Sr by Ca in Sr_2RuO_4 has a great impact onto magnetic properties of the system despite that the number of carriers remains intact. The RuO_6 octahedra rotation affects strongly the electronic structure providing the electronic topological transition in the γ band[9] with Fermi level passing through the van Hove singularity. This is accompanied by a number of magnetic anomalies for the Fermi level below VHS (after an appropriate particle-hole transformation): divergence of the Wilson ratio and magnetic susceptibility in $Ca_{1.5}Sr_{0.5}RuO_4$,[11] incommensurate magnetic fluctuations of a new type in $Ca_{1.8}Sr_{0.2}RuO_4$ and $Ca_{1.38}Sr_{0.62}RuO_4$, which are most likely produced by the γ band.[12]

Bilayer ruthenate compound $Sr_3Ru_2O_7$ also provides a number of interesting physical properties, in particular, incommensurate magnetic fluctuations[13] and metamagnetism.[14–16] The effect of substitution of Sr by Ca in $(Sr_{1-x}Ca_x)_3Ru_2O_7$ was studied in Ref. 17. Although the Wilson ratio approaches $\sim$700 for $x = 0.2$, and the system becomes nearly ferromagnetic in the temperature interval ($3 \lesssim T \lesssim 10$ K), further lowering of temperature does not result in the long-range ferromagnetic ordering, but instead forces the system to freeze into a spin-glass state.

Therefore, an important problem related to the magnetic properties of metallic two-dimensional compounds is revealing the conditions for which the ferromagnetic order (observed to be suppressed experimentally) is stable. To investigate an interplay of different magnetic states in itinerant layered systems, it is convenient to consider the two-dimensional (2D) one-band Hubbard model. It is justified by ARPES experiments and

first-principles calculations of the above-mentioned compounds that the electronic spectrum is quasi-two-dimensional and can be fit using nearest-(t) and next-nearest-neighbor (t') hoppings. Despite the fact that this model is strongly simplified as compared to the situation in real compounds, it catches an important dependence of ground-state ordering on the form of the electronic spectrum, in particular, on the t'/t ratio and band filling. On the other hand, the electronic spectrum containing nearest-neighbor and next-nearest-neighbor hoppings retains VHS, which is often present in the density of states (DOS) of real compounds.

A large enough value of DOS at the Fermi level, occurring due to VHS, leads to the ferromagnetic ground state according to the Stoner theory.[18] This approach, however, neglects magnetic fluctuations, in particular, of incommensurate type. A generalization of the Stoner theory to treat the spin spiral instability and Néel antiferromagnetism reveals that, in a major part of the phase diagram, the spiral phase is even more preferable than the ferromagnetic one.[19,20] In particular, the phases with the wave vectors $\mathbf{Q} = (Q, Q)$ and $\mathbf{Q} = (Q, \pi)$ were found to compete strongly with the ferromagnetic phase.[20] The critical value of the Hubbard interaction U_c for the ferromagnetic instability is smallest in the region with the Fermi level below VHS. On the other hand, in the vicinity and well above VHS, the ferromagnetic phase is to a great extent suppressed by the incommensurate (Q, Q) phase.

These results are also supported by studies of the 2D *spin-fermion* model,[21] which show that the competition with incommensurate magnetic fluctuations results in substantial shrinkage of the region of stability of ground-state ferromagnetism in comparison with Stoner theory in qualitative agreement with the mean field for incommensurate phases[20] and variational results.[22] A T-matrix approximation[23] may serve as a natural addition to the consideration based on the spin-fermion model treating the particle-particle contribution and being exact in the limit of a small number of carriers, although the possibility of incommensurate magnetic ordering was missed by this approximation. The above-discussed approaches neglect the effects of the renormalization of electronic spectrum, although the consideration within the spin fermion treats incoherent contributions to the electronic Green's function yielding quasisplitting of the Fermi surface at low temperatures for the ferromagnetic ground state.[24] These renormalizations can be important for the condition of magnetic instabilities.

To study interplay of magnetic and electronic properties and their effect on the possibility of ferromagnetic instability, we focus here on the functional renormalization-group (fRG) technique, which is a powerful tool for treatment of correlation effects (see Ref. 25 for the introduction in the application to the Hubbard model). In the pioneering study of Ref. 26, the use of the Polchinski's form of fRG technique allowed us to construct the phase diagram of the nearest-neighbor-hopping Hubbard model (μ-T plane). The momentum cutoff scheme of the Wick-ordered version of fRG equations was employed to obtain the ground-state instability type at small t'/t in Ref. 27. Later, the temperature[28–30] and Hubbard interaction[31] were used as flow parameters in one-particle irreducible (1PI) investigations of the t-t' Hubbard model. The main result of these studies is that the small next-nearest-neighbor hopping ($t'/t \leqslant 0.2$) favors the antiferromagnetic instability at VH filling, the moderate next-nearest-neighbor hopping ($0.2 \leqslant t'/t \leqslant 0.35$) favors the d-wave supeconducting instability, and the rather large $t'/t > 0.35$ corresponds to ferromagnetic instability. Away from van Hove band filling, the competition of antiferromagnetic and superconducting instabilities is obtained at small t'/t, while at larger values $t'/t \gtrsim 0.35$, the competition of ferromagnetic instability and p-wave superconductivity is observed.[28,29,31]

The essential shortcoming of the above-reviewed approaches[27–29,31] is that these do not consider the self-energy corrections to the electronic Green's function. Hence, important nontrivial effects of renormalization of the electronic spectrum in the vicinity of magnetic phase transition (or in the regime with strong magnetic fluctuations) can be missed, provided that the Fermi level is near VHS. On the other hand, spin-dependent self-energy corrections provide the mechanism of the response to magnetic field, which is crucial in the context of investigation of ferromagnetic instability. Note that only antiferromagnetic and superconducting phases were considered previously within the combination of fRG and mean-field approaches (Ref. 32), and within the fRG approach in the symmetry broken phase.[33] Considering ferromagnetic instability poses a problem of scale-dependent FS, which was theoretically elaborated only in the self-adjusting Polchinski and Wick-ordered schemes, proposed in Ref. 34.

In this paper, we present a study of the evolution of magnetic and electronic properties with decreasing temperature within 1PI fRG in zero and small finite magnetic fields. We treat accurately the FS problem, including movement of projecting points and momentum dependence of the self-energy. The plan of this paper is the following. In Sec. II, we introduce the model and review earlier approaches to ferromagnetic instability at weak and intermediate coupling. In Sec. III, we introduce the details of our fRG approach to take into account the fluctuation effects, retaining the electronic self-energy. In Sec. IV, we present and discuss the numerical results. In Sec. V, we present the conclusions.

II. THE MODEL AND EARLIER APPROACHES

We consider the Hubbard model with the action

$$\mathcal{S} = \beta \sum_{k\sigma} (-\mathrm{i}\nu_n + \epsilon_{\mathbf{k}} - \mu - h\sigma) c^+_{k\sigma} c_{k\sigma} + \frac{\beta U}{4N} \sum_{k_1 k_2 k_3 k_4 \sigma\sigma'} c^+_{k_1\sigma} c^+_{k_2\sigma'} c_{k_3\sigma'} c_{k_4\sigma} \delta_{k_1+k_2,k_3+k_4}, \quad (1)$$

where $\beta = 1/T$ is inverse temperature, N is the number of lattice sites, h is a magnetic field directed along the z axis (measured in units of Bohr magneton), $\epsilon_{\mathbf{k}}$ is an electronic spectrum, μ is the chemical potential, U is the Hubbard on-site interaction, and δ is the Kronecker δ symbol. The sums in Eq. (1) are taken over 4-vectors $k = (\mathrm{i}\nu_n, \mathbf{k})$, where $\nu_n = \pi(2n+1)T$ are the fermionic Matsubara frequencies ($n \in \mathbb{Z}$). We consider electronic dispersion on the square lattice

$$\epsilon_{\mathbf{k}} = -2t(\cos k_x + \cos k_x) + 4t'(\cos k_x \cos k_y + 1), \quad (2)$$

where $t,t' > 0$ are hopping parameters. Such a form of the spectrum corresponds to VHS at zero energy. We fix the ratio $t'/t = 0.45$.

To gain insight into possible types of magnetic order, we consider the magnetic susceptibility $\chi_{\mathbf{q}}(\omega)$ in the paramagnetic state[35]

$$\chi_{\mathbf{q}}^{-1}(\omega) = \phi_{\mathbf{q}}^{-1}(\omega) - U, \tag{3}$$

where $\phi_{\mathbf{q}}(\omega)$ is the susceptibility, irreducible in the particle-hole channel. The paramagnetic state is unstable with respect to the formation of the incommensurate state with the wave vector $\mathbf{Q}$, provided that the maximum of irreducible susceptibility $\phi_{\mathbf{q}}(0)$ is at $\mathbf{q} = \mathbf{Q}$ and $\chi_{\mathbf{Q}}(0)$ diverges. A critical interaction for stability of such an incommensurate magnetic state $U_c = \phi_{\mathbf{Q}}^{-1}(0)$. For the sake of simplicity, let us consider the random-phase approximation (RPA) where $\phi_{\mathbf{q}}(\omega)$ coincides with the noninteracting spin susceptibility

$$\chi_{\mathbf{q}}^{0}(\mathrm{i}\omega_n) = -\frac{T}{N}\sum_{\mathbf{k}\nu_n} G_{\mathbf{k}}^{0}(\mathrm{i}\nu_n) G_{\mathbf{k}+\mathbf{q}}^{0}(\mathrm{i}\nu_n + \mathrm{i}\omega_n), \tag{4}$$

where $G_{\mathbf{k}}^{0}(\mathrm{i}\nu_n) = (\mathrm{i}\nu_n - \epsilon_{\mathbf{k}} + \mu)^{-1}$ is the noninteracting electronic Green's function. In Fig. 1, we present the zero-temperature momentum profile of static noninteracting magnetic susceptibility $\chi_{\mathbf{q}}^{0}(\omega = 0)$. Below VH filling, the competition between incommensurate magnetic structure with large wave vector and a variety of incommensurate instabilities with small magnetic wave vectors is observed [see Fig. 1(a)]. On the other hand, above VH filling, the ferromagnetic instability competes with the long-wave incommensurate magnetic instability[21] [see Fig. 1(b)]. This consideration shows that, for large enough t', the tendency to incommensurate magnetic ordering originates from the geometry of the FS.

The competition of ferromagnetism and incommensurate magnetic ordering beyond mean-field approximation was discussed within the quasistatic approach (QSA) in Ref. 21. Under the assumption of the ground state to be ferromagnetically ordered, it was found that magnetic fluctuations can reconstruct the momentum dependence of the susceptibility only at finite electronic interaction, stabilizing the ferromagnetic ground state with respect to incommensurate magnetic fluctuations. Above the critical value of the interaction, the maximum of $\phi_{\mathbf{q}}(0)$ is reached at $\mathbf{q} = \mathbf{0}$. The corresponding result for the boundary separating the ferromagnetic and (Q,Q) incommensurate instabilities is presented below in Fig. 10.

The effort of direct account of the electron correlation effects was performed in temperature-flow fRG study[28,29] ($\Sigma = 0$ fRG). While the problem of ferromagnetism formation was investigated in zero magnetic field, the self-energy renormalization was neglected, which makes the FS scale independent and the chemical potential not renormalized. Formal consequences of this assumption are discussed in Sec. III D.

III. FUNCTIONAL RENORMALIZATION GROUP WITH SELF-ENERGY CORRECTIONS

This paper is an extension of the study of Ref. 29. Contrary to previous approaches, (i) we do not neglect the self-energy corrections Σ to the electronic Green's function G and account for their momentum dependence, which results in the renormalization of spectrum parameters t and t' and moving FS, and (ii) we partially take into account the momentum dependence of the vertex inside the patches, which allows us to account for the scale dependence of the Fermi surfaces $\mathcal{F}_\sigma(s)$, corresponding to different spin projections $\sigma = \pm 1$.

A. fRG equations

We use the 1PI fRG equations[25] in the truncation of Ref. 36:

$$\dot{\Gamma} = \Gamma * \frac{d}{ds}(G_s G_s) * \Gamma\Big|_{\mathrm{pp}} + \Gamma * \frac{d}{ds}(G_s G_s) * \Gamma\Big|_{\mathrm{ph}} + \Gamma * \frac{d}{ds}(G_s G_s) * \Gamma\Big|_{\mathrm{ph1}}, \tag{5}$$

$$\dot{\Sigma}_s = \Gamma * S, \tag{6}$$

where Γ is the 1PI 4-vertex function (we refer to it as a vertex below); pp, ph, and ph1 denote particle-particle and two independent particle-hole channels; $S = -G_s^2 dG_{0,s}^{-1}/ds$ is the single-scale propagator; and $G_{0,s}$, G_s, and Σ_s are the appropriately rescaled noninteracting and interacting Green's

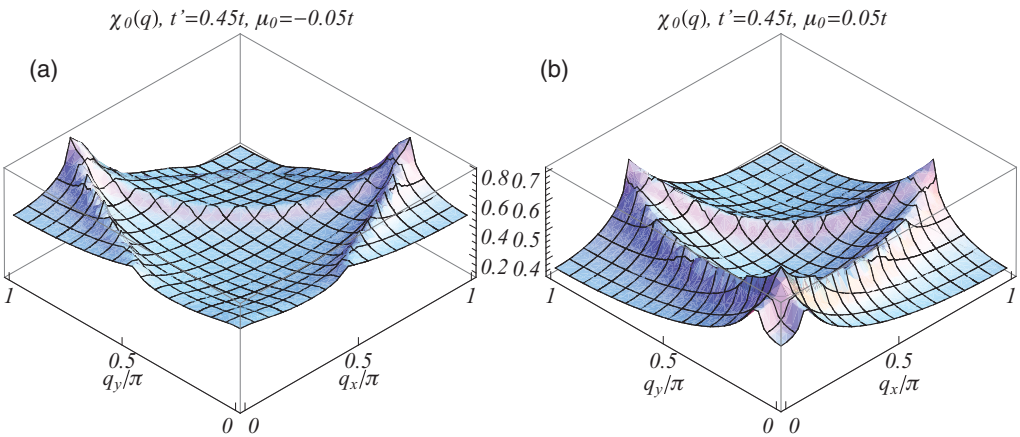

FIG. 1. (Color online) Momentum dependence of the static magnetic susceptibility of free electrons $\chi_{\mathbf{q}}^{0}(\omega = 0)$, $t' = 0.45t$: (a) Fermi level below VH filling ($\mu = -0.05t$); (b) Fermi level above VH filling ($\mu = 0.05t$).

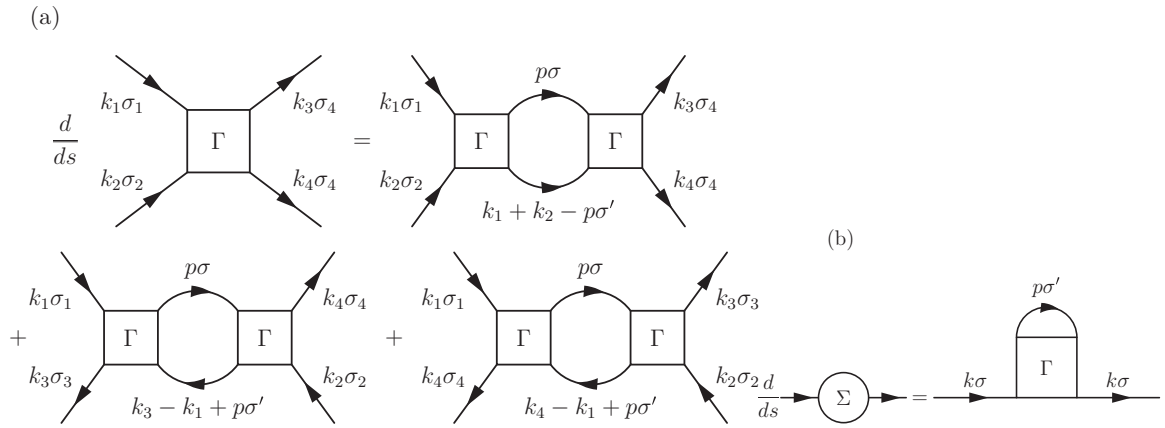

FIG. 2. Diagrammatic representation of (a) Eqs. (5) and (10) and (b) Eqs. (6) and (11). Pairs of internal lines in (a) correspond to scale derivative of particle-particle and particle-hole bubbles [see Eqs. (12) and (13)]. Internal line in (b) denotes the single-scale propagator S.

functions and the self-energy, respectively. Momentum arguments and spin indices are omitted for brevity. The asterisks denote the summation over internal 4-momentum and spin indices corresponding to a specified channel, and the dots denote the derivatives, taken with respect to the scale parameter s. Equations (5) and (6) are shown diagrammatically in Fig. 2.

If ferromagnetic (FM) order parameter or magnetic field are directed along the z axis, the SU(2) symmetry is broken. The remaining axial symmetry results in the self-energy, which is diagonal in spin indices σ,σ':

$$\Sigma_{\sigma\sigma'}(k) = \Sigma_{k\sigma}\delta_{\sigma\sigma'}, \tag{7}$$

and the vertex function components are nonzero provided that $\sigma_1 + \sigma_2 = \sigma_3 + \sigma_4$. We consider the vertex component $\Gamma_{\sigma_1\sigma_2;\sigma_1\sigma_2}$ (for brevity, we denote it as $\Gamma_{\sigma_1\sigma_2}$); the others can be obtained using the exact relation

$$\begin{aligned}\Gamma_{\sigma_1\sigma_2;\sigma_3\sigma_4}(k_1,k_2;k_3,k_4) &= -\Gamma_{\sigma_2\sigma_1;\sigma_3\sigma_4}(k_2,k_1;k_3,k_4)\\ &= \Gamma_{\sigma_2\sigma_1;\sigma_4\sigma_3}(k_2,k_1;k_4,k_3).\end{aligned} \tag{8}$$

Another useful property, which is a consequence of the symmetry with respect to the combination of time-reversal transformation and $\sigma \to -\sigma$ transformation, is

$$\Gamma_{\sigma_1\sigma_2;\sigma_3\sigma_4}(k_1,k_2;k_3,k_4) = \bar{\Gamma}_{\sigma_3\sigma_4;\sigma_1\sigma_2}(k_3,k_4;k_1,k_2). \tag{9}$$

By neglecting the frequency dependence of the vertex and self-energy, the fRG equations can be written in the following explicit form:

$$\begin{aligned}\dot{\Gamma}_{\sigma_1\sigma_2}(\mathbf{k}_1,\mathbf{k}_2;\mathbf{k}_3,\mathbf{k}_4) = {}& \big(1-\delta_{\sigma_1\sigma_2}/2\big)\frac{1}{N}\sum_{\mathbf{p}}\Gamma_{\sigma_1\sigma_2}(\mathbf{k}_1,\mathbf{k}_2;\mathbf{p},\mathbf{k}_1+\mathbf{k}_2-\mathbf{p})\mathcal{L}^{\mathrm{pp}}_{\sigma_1\sigma_2}(\mathbf{p},\mathbf{k}_1+\mathbf{k}_2-\mathbf{p})\Gamma_{\sigma_1\sigma_2}(\mathbf{p},\mathbf{k}_1+\mathbf{k}_2-\mathbf{p};\mathbf{k}_3,\mathbf{k}_4)\\ &- \frac{1}{N}\sum_{\mathbf{p}\sigma}\Gamma_{\sigma_1\sigma}(\mathbf{k}_1,\mathbf{p};\mathbf{k}_3,\mathbf{k}_1-\mathbf{k}_3+\mathbf{p})\mathcal{L}^{\mathrm{ph}}_{\sigma\sigma}(\mathbf{p},\mathbf{k}_1-\mathbf{k}_3+\mathbf{p})\Gamma_{\sigma\sigma_2}(\mathbf{k}_1-\mathbf{k}_3+\mathbf{p},\mathbf{k}_2;\mathbf{p},\mathbf{k}_4)\\ &+ \delta_{\sigma_1\sigma_2}\frac{1}{N}\sum_{\mathbf{p}\sigma}\Gamma_{\sigma_1\sigma}(\mathbf{k}_1,\mathbf{k}_2-\mathbf{k}_3+\mathbf{p};\mathbf{k}_4,\mathbf{p})\mathcal{L}^{\mathrm{ph}}_{\sigma\sigma}(\mathbf{p},\mathbf{k}_2-\mathbf{k}_3+\mathbf{p})\Gamma_{\sigma\sigma_2}(\mathbf{p},\mathbf{k}_2;\mathbf{k}_2-\mathbf{k}_3+\mathbf{p},\mathbf{k}_3)\\ &+ \big(1-\delta_{\sigma_1\sigma_2}\big)\frac{1}{N}\sum_{\mathbf{p}}\Gamma_{\sigma_1\sigma_2}(\mathbf{k}_1,\mathbf{k}_2-\mathbf{k}_3+\mathbf{p};\mathbf{p},\mathbf{k}_4)\mathcal{L}^{\mathrm{ph}}_{\sigma_1\sigma_2}(\mathbf{p},\mathbf{k}_2-\mathbf{k}_3+\mathbf{p})\Gamma_{\sigma_1\sigma_2}(\mathbf{p},\mathbf{k}_2;\mathbf{k}_3,\mathbf{k}_2-\mathbf{k}_3+\mathbf{p}),\end{aligned} \tag{10}$$

$$\dot{\Sigma}_{\mathbf{k}\sigma} = \frac{1}{2N}\sum_{\mathbf{p}\sigma'}\Gamma_{\sigma\sigma'}(\mathbf{k},\mathbf{p};\mathbf{k},\mathbf{p})\big[f_{\mathbf{p}\sigma'} + (2\varepsilon_{\mathbf{p}\sigma'} - \Sigma_{\mathbf{p}\sigma'})f'_{\mathbf{p}\sigma'}\big] - \dot{\mu}\sum_{\mathbf{p}\sigma'}\Gamma_{\sigma\sigma'}(\mathbf{k},\mathbf{p};\mathbf{k},\mathbf{p})f'_{\mathbf{p}\sigma'} - \Sigma_{\mathbf{k}\sigma}/2, \tag{11}$$

where

$$\mathcal{L}^{\mathrm{pp}}_{\sigma\sigma'}(\mathbf{k},\mathbf{k}') = \left[\frac{\varepsilon_{\mathbf{k}\sigma}f'_{\mathbf{k}\sigma} + \varepsilon_{\mathbf{k}'\sigma'}f'_{\mathbf{k}'\sigma'}}{\varepsilon_{\mathbf{k}\sigma} + \varepsilon_{\mathbf{k}'\sigma'}} + \frac{\big(\dot{\Sigma}_{\mathbf{k}\sigma} - \dot{\mu}\big)f'_{\mathbf{k}\sigma} + \big(\dot{\Sigma}_{\mathbf{k}'\sigma'} - \dot{\mu}\big)f'_{\mathbf{k}'\sigma'}}{\varepsilon_{\mathbf{k}\sigma} + \varepsilon_{\mathbf{k}'\sigma'}} - \frac{(f_{\mathbf{k}\sigma} + f_{\mathbf{k}'\sigma'} - 1)\big(\dot{\Sigma}_{\mathbf{k}\sigma} + \dot{\Sigma}_{\mathbf{k}'\sigma'} - 2\dot{\mu}\big)}{(\varepsilon_{\mathbf{k}\sigma} + \varepsilon_{\mathbf{k}'\sigma'})^2}\right], \tag{12}$$

$$\mathcal{L}^{\mathrm{ph}}_{\sigma\sigma'}(\mathbf{k},\mathbf{k}') = -\left[\frac{\varepsilon_{\mathbf{k}\sigma}f'_{\mathbf{k}\sigma} - \varepsilon_{\mathbf{k}'\sigma'}f'_{\mathbf{k}'\sigma'}}{\varepsilon_{\mathbf{k}\sigma} - \varepsilon_{\mathbf{k}'\sigma'}} + \frac{\big(\dot{\Sigma}_{\mathbf{k}\sigma} - \dot{\mu}\big)f'_{\mathbf{k}\sigma} - \big(\dot{\Sigma}_{\mathbf{k}'\sigma'} - \dot{\mu}\big)f'_{\mathbf{k}'\sigma'}}{\varepsilon_{\mathbf{k}\sigma} - \varepsilon_{\mathbf{k}'\sigma'}} - \frac{(f_{\mathbf{k}\sigma} - f_{\mathbf{k}'\sigma'})\big(\dot{\Sigma}_{\mathbf{k}\sigma} - \dot{\Sigma}_{\mathbf{k}'\sigma'}\big)}{(\varepsilon_{\mathbf{k}\sigma} - \varepsilon_{\mathbf{k}'\sigma'})^2}\right]. \tag{13}$$

We have introduced the renormalized electronic spectrum

$$\varepsilon_{\mathbf{k}\sigma} = \epsilon_{\mathbf{k}} - \mu - h\sigma + \Sigma_{\mathbf{k}\sigma}, \tag{14}$$

and $f_{\mathbf{p}\sigma} \equiv f(\varepsilon_{\mathbf{p}\sigma}) = \frac{1}{2}[1 - \tanh(\beta\varepsilon_{\mathbf{p}\sigma}/2)]$. Note that the neglect of the frequency dependence of the vertex function Γ and the self-energy Σ necessary implies the vanishing of $\mathrm{Im}\Sigma$ and $\mathrm{Im}\Gamma$, which leaves incoherent contributions to the Green's function beyond the scope of the present consideration. This is justified at not too low temperatures where the quasiparticle concept is valid and the quasisplitting of the Fermi surface[24] is absent.

Below, we consider the temperature cutoff[28] with $s = \log(t/T)$. The single-scale propagator has the form

$$S^T_{k\sigma} = -G^2_{k\sigma}\left(\frac{i\nu_n - \epsilon_{\mathbf{k}} - h\sigma + \mu}{2T^{1/2}} + T^{1/2}\frac{d\mu}{dT}\right), \tag{15}$$

where $G_{k\sigma} = (i\nu_n - \varepsilon_{\mathbf{k}\sigma})^{-1}$. In this paper, we choose temperature-independent bare chemical potential ($d\mu/dT = 0$), although the temperature dependence of μ can be adjusted, e.g., to keep the number of particles fixed.[37] Equations (10) and (11) are basic for the 1PI fRG approach since they can, in principle, determine the renormalization of the electronic spectrum and interaction at any temperature. This system of equations should be supplemented by initial conditions at $s = -\infty(T = +\infty)$. In the infinite-temperature limit, correlation effects are absent, and one obtains for the self-energy $\Sigma_{\mathbf{k}\sigma} = U/2$ and interaction $\Gamma_{\sigma_1\sigma_2}(k_1,k_2;k_3,k_4) = U(1 - \delta_{\sigma_1\sigma_2})$.

The fRG equations (10) and (11) form the system of ordinary *functional* differential equations. To solve them numerically, one has to introduce some approximation procedure to reduce the considered system to a finite system of ordinary equations. Below, we present the procedure of numerical solution in details.

B. The self-energy ansatz and Fermi surface

The first step is the use of common patching scheme[28] to avoid dealing with the system of functional equations. However, we do not neglect the momentum dependence of the self-energy (and vertices) inside the patches, in particular, Eq. (11) is fully employed. We assume that the self-energy has the form

$$\Sigma_{\mathbf{k}\sigma} = -2\delta t_\sigma(\cos k_x + \cos k_y) + 4\delta t'_\sigma \cos k_x \cos k_y + \Sigma_\sigma, \tag{16}$$

where the parameters $\delta t_\sigma, \delta t'_\sigma$, and Σ_σ are determined as follows. While solving numerically the system of fRG equations, at each step, we calculate the values of $\dot{\Sigma}_{\mathbf{k}\sigma}$ on two sets of (σ-dependent) projecting points (PPs, see the Appendix for details). For considered $\mathbf{k} \in$ PPs, the linear regression procedure is used:

$$\dot{\Sigma}_{\mathbf{k}\sigma} \to -2\delta\dot{t}_\sigma(\cos k_x + \cos k_y) + 4\delta\dot{t}'_\sigma \cos k_x \cos k_y + \dot{\Sigma}_\sigma. \tag{17}$$

In this way, we determine the flow of unknown quantities $\delta t_\sigma, \delta t'_\sigma$, and Σ_σ in Eqs. (10) and (11).

Such a choice efficiently reduces the number of variables and retains VHS points of the renormalized spectrum. Note that Σ_σ does not depend on $\mathbf{k}$ and renormalizes the chemical potential μ; δt_σ and $\delta t'_\sigma$ contribute to the change of momentum dependence of the spectrum (δt_σ corresponds to the bandwidth renormalization).

Therefore, it is convenient to represent the renormalized spectrum (14) in the form

$$\begin{aligned}\varepsilon_{\mathbf{k}\sigma} = {} & -2t_{\mathrm{eff},\sigma}(\cos k_x + \cos k_x) \\ & + 4t'_{\mathrm{eff},\sigma}(\cos k_x \cos k_y + 1) - \mu_{\mathrm{eff},\sigma},\end{aligned} \tag{18}$$

where

$$\begin{aligned}\mu_{\mathrm{eff},\sigma} &= \mu - \Sigma_\sigma + 4\delta t'_\sigma + h\sigma, \\ t_{\mathrm{eff},\sigma} &= t + \delta t_\sigma t'_{\mathrm{eff},\sigma} = t' + \delta t'_\sigma.\end{aligned} \tag{19}$$

The scale-dependent effective chemical potential $\mu_{\mathrm{eff},\sigma}$ results in Fermi surface, calculated with the renormalized spectrum parameters $t_{\mathrm{eff},\sigma}, t'_{\mathrm{eff},\sigma}$. Applying the present method, one should be careful in determining the geometry of the FS. If $t'_{\mathrm{eff},\sigma}/t_{\mathrm{eff},\sigma} < 1/2$, the bottom of the band is at the energy $w_\sigma = -4t_{\mathrm{eff},\sigma} + 8t'_{\mathrm{eff},\sigma}$ and the FS is singly connected; however, if $t'_{\mathrm{eff},\sigma}/t_{\mathrm{eff},\sigma} \geqslant 1/2$, the bottom of the band is zero. In this case, if $\mu_{\mathrm{eff},\sigma} \geqslant w_\sigma$, the FS is singly connected and the patching scheme of Ref. 26 can be used, while for $\mu_{\mathrm{eff},\sigma} < w_\sigma$, the Fermi surface consists of two disconnected parts and the patching scheme should be chosen differently.

Despite that the self-energy renormalization is included in this study, we neglect incoherent contributions to the Green's functions. Due to this renormalization, the actual Fermi level μ_{eff} is determined by the combination of the bare spectrum and the self-energy parameters (19) at the end of the flow.

C. The vertex ansatz

The vertex function Γ is represented by its values at the current FS. Since we always trace the renormalization of $\Sigma_{\mathbf{k}\sigma}$, we have to take into account moving of the Fermi surface during fRG flow. PPs of the current FS are changing during the flow and the discrete (projected) vertex function derivative acquires an additional contribution corresponding to this movement,

$$\frac{d\Gamma}{ds} = \frac{\partial\Gamma}{\partial s} + \frac{\partial\Gamma}{\partial k_{\mathrm{PP}}}\frac{dk_{\mathrm{PP}}}{ds}. \tag{20}$$

We denote symbolically the derivatives with respect to PPs (k_{PP}) as $\partial/\partial k_{\mathrm{PP}}$.

To take into account this momentum dependence of Γ, we assume that, apart from the position of external legs in certain patches, the vertex function depends on momenta $\mathbf{k}_i$ through the renormalized energies $\varepsilon_{\mathbf{k}_i\sigma}$ and linearize the latter dependence. Let the momenta of external legs $\mathbf{k}^{\mathrm{c}}_1, \mathbf{k}^{\mathrm{c}}_2, \mathbf{k}^{\mathrm{c}}_3$ be on the current FS and consider vertex with all momenta $\mathbf{k}_i$ belonging to the main set of PPs and three vertices with two momenta $\mathbf{k}_i$ belonging to the main set of PPs (see Appendix), and one belonging to the auxiliary set. Therefore, we have four possibilities for the choice of $\mathbf{k}_1, \mathbf{k}_2, \mathbf{k}_3$, and obtain a system of four linear equations (we use $\varepsilon_{\mathbf{k}^{\mathrm{c}}_i\sigma_i} = 0$)

$$\begin{aligned}&\Gamma_{\sigma\sigma'}(\mathbf{k}^{\mathrm{c}}_1, \mathbf{k}^{\mathrm{c}}_2; \mathbf{k}^{\mathrm{c}}_3) + \sum_i \partial_i \Gamma_{\sigma\sigma'}(\mathbf{k}^{\mathrm{c}}_1, \mathbf{k}^{\mathrm{c}}_2; \mathbf{k}^{\mathrm{c}}_3)\varepsilon_{\mathbf{k}_i\sigma_i} \\ &\quad = \Gamma_{\sigma\sigma'}(\mathbf{k}_1, \mathbf{k}_2; \mathbf{k}_3),\end{aligned} \tag{21}$$

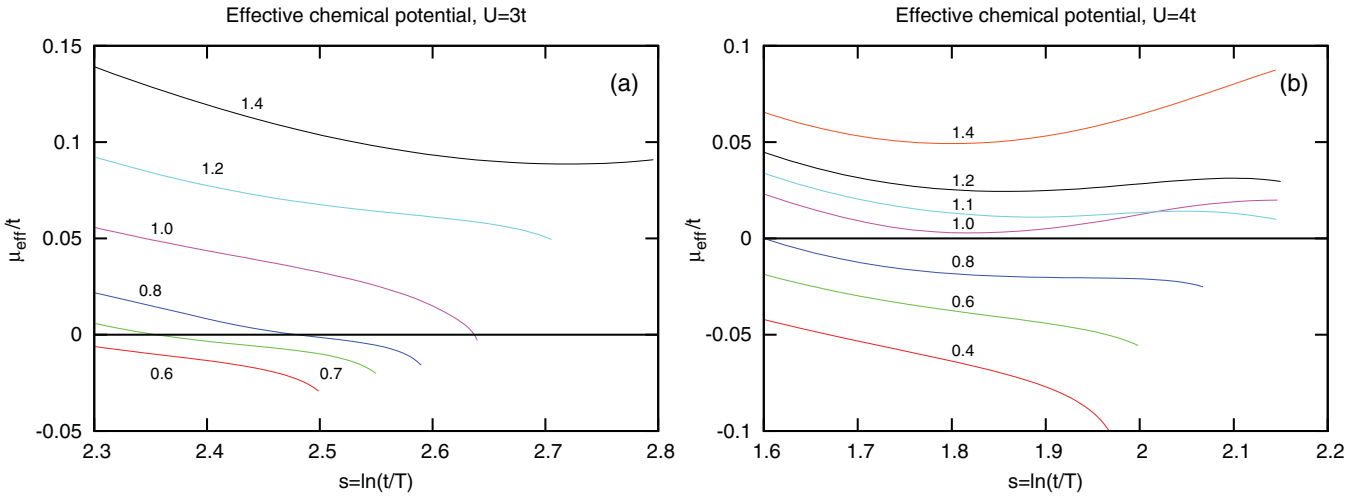

FIG. 3. (Color online) Temperature dependence of the renormalized Fermi level $\mu_{\rm eff}$ at $h = 0$: (a) $U = 3t$, (b) $U = 4t$. Chemical potential values $\bar{\mu}$ (see text) are shown by numbers near the plots.

with unknown quantities $\Gamma_{\sigma\sigma'}(\mathbf{k}_1^c,\mathbf{k}_2^c;\mathbf{k}_3^c)$ and $\partial_i\Gamma_{\sigma\sigma'}(\mathbf{k}_1^c,\mathbf{k}_2^c;\mathbf{k}_3^c)$. Solving the system (21) one determines the vertex on the current FS.

D. Relation to previous approaches

In the zero magnetic field, neglecting the momentum dependence of the self-energy (i.e., with $\delta t = \delta t' = 0$), one can demand the chemical potential to absorb all the corrections to the self-energy in Eq. (10), which is possible since the electronic spectrum enters Eq. (10) through $\varepsilon_{\mathbf{k}\sigma}$ only. On the other hand, Eq. (11), being reformulated with $\mu' = \mu - \Sigma$, reduces to $\dot{\mu}' = 0$. Hence, in this case, μ is replaced by a constant μ'. The important consequence of this approximation is that FS is fixed within this ansatz since it is determined solely by the scale-independent parameter μ'.

If the field is nonzero, the self-energy corrections can not be absorbed into the chemical potential even when the renormalization of the hopping parameters is neglected. This, in turn, results in moving of spin FSs during the flow so that the projected vertex acquires a contribution from this moving. As described in detail in Sec. III C, we account for this contribution in the self-consistent numerical scheme of treatment of Eqs. (10), (11), and (21).

IV. TEMPERATURE DEPENDENCE OF THE RENORMALIZED PARAMETERS

In this section, we present and discuss numerical results of the present fRG approach accounting for the self-energy corrections in zero (Sec. IV A) and finite magnetic fields (Sec. IV B). Afterward, in Sec. IV C, we present our results for the phase diagram.

A. Results in zero magnetic field

In this section, we consider the results of fRG calculations in the spin symmetric phase for $U/t = 3$ and 4. We choose the bare chemical potential μ in such a way that, at the end of the flow, the renormalized position of the Fermi level $\mu_{\rm eff}$, determined by Eq. (19), lies in the vicinity of VHS. It is clear physically and verified numerically in our investigation that the magnetic response is suppressed for the Fermi level well separated from VHS.

Starting from an infinite-temperature limit, the position of the Fermi level first tends to increase from its high-temperature Hartree value $\mu - U/2$ to almost low-temperature Hartree value $\bar{\mu} = \mu - U\int_{-4t+8t'}^{\bar{\mu}}\rho(\varepsilon)d\varepsilon$, with ρ being the bare DOS. At even lower temperatures, μ decreases due to correlation effects. The obtained low-temperature scale dependence of $\mu_{\rm eff}$ for different bare chemical potentials μ is shown in Figs. 3(a) ($U/t = 3$) and 3(b) ($U/t = 4$). We stop the flow when the effective interaction becomes too large ($\gtrsim 2.5W$, where $W = 8t$ is bare bandwidth). The corresponding scale $s_{\rm min}$ yields the minimal temperature that is available within the flow $T_{\rm min} = t\exp(-s_{\rm min})$. In the following, we parametrize the initial chemical potential of the flow by the Hartree Fermi level $\bar{\mu}$.

The cases $U = 3t$ and $4t$ are somewhat different due to the absence of the region of saturation of $\mu_{\rm eff}(s)$ dependence for $U = 3t$, although the dependence $\mu_{\rm eff}(s)$ becomes weak at the end of the flow. Below, we consider the renormalized Fermi level $\mu_{\rm eff}$ in the saturation region (if it exists) as a representative parameter that characterizes the flow, since the renormalization of other parameters of the electronic spectrum is not too strong. The charge response is slightly suppressed in the vicinity of van Hove filling for the case $\mu_{\rm eff} < 0$ more than for $\mu_{\rm eff} > 0$. The nonmonotonous behavior of $\mu_{\rm eff}(s)$ slightly above VHS ($\bar{\mu} = 1.0t$) for $U = 4t$ (of which consequences are discussed below) is worthy of notice.

In our scheme, the effective chemical potential renormalization has substantial contribution from t and t' renormalizations [see Eq. (19)]. In Fig. 4, we present, for instance, $t_{\rm eff}/t$ and $t'_{\rm eff}/t_{\rm eff}$ plots for $U = 4t$. The bandwidth ($t_{\rm eff}/t$) is somewhat reduced at the end of the flow well below VHS, indicating prominent correlation effects; for $\mu_{\rm eff}$ above VHS, $t_{\rm eff}/t$ first increases with decreasing temperature (which implies that correlation effects in this regime are not substantial)

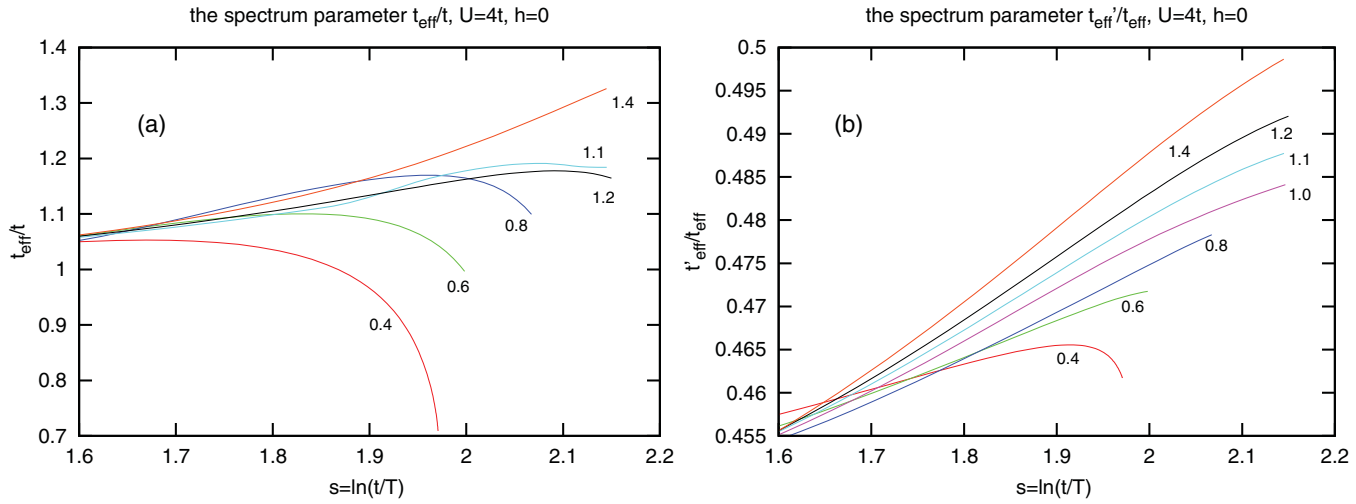

FIG. 4. (Color online) Effective (renormalized) hopping parameters: (a) $t_{\rm eff}/t$, (b) $t'_{\rm eff}/t_{\rm eff}$ for $U = 4t$. Numbers correspond to the value of chemical potential $\bar{\mu}$.

and then decreases at lower temperatures, which is related to enhancement of the vertex in the vicinity of magnetic instability. On the other hand, the ratio t'/t is not strongly renormalized (this means that the self-energy effects do not change substantially the curvature of the Fermi surface) and monotonously increases toward the value $1/2$ as $\bar{\mu}$ increases, which corresponds to flattening of the electronic dispersion. The complete treatment of the case $\bar{\mu} \geqslant 1.4t$, where $t'_{\rm eff}/t_{\rm eff}$ exceeds $1/2$ during the flow, corresponding to a change of FS geometry (see for details Sec. III B), requires special consideration and is beyond the scope of this paper.

The type of leading magnetic instability can be inferred from the behavior of vertices. Let us consider the scale profiles of the maximal vertex. We consider the maximal total vertex $\Gamma^{\rm max}_{\uparrow\downarrow}$ (the maximum is taken over all possible combinations of momenta) and maximal exchange vertex $\Gamma^{\rm max,E}_{\uparrow\downarrow}$ (the maximum is taken over all combinations of momenta with $\mathbf{k}_2 = \mathbf{k}_3$). The ferromagnetic instability is accompanied by coincidence of $\Gamma^{\rm max}_{\uparrow\downarrow}$ and $\Gamma^{\rm max,E}_{\uparrow\downarrow}$ in the vicinity of transition point where both the values diverge, reflecting an instability of the paramagnetic state with respect to zero-momentum collective spin excitations. Therefore, the criterion for commensurate magnetic fluctuations has the form

$$\Delta\Gamma_{\rm max} \equiv \Gamma^{\rm max}_{\uparrow\downarrow} - \Gamma^{\rm max,E}_{\uparrow\downarrow} = 0 \qquad (22)$$

and yields information about the type of leading instability.

The scale dependences of $\Gamma^{\rm max}_{\uparrow\downarrow}$ and $\Gamma^{\rm max,E}_{\uparrow\downarrow}$ for different $\bar{\mu}$ are presented in Figs. 5 ($\mu_{\rm eff} < 0$) and 6 ($\mu_{\rm eff} > 0$). Let us consider first the case of Fermi level below VHS, $\mu_{\rm eff} < 0$. For both the cases $U = 3t$ [Fig. 5(a)] and $U = 4t$ [Fig. 5(b)], $\Gamma^{\rm max}_{\uparrow\downarrow}$ is diverging and $\Delta\Gamma_{\rm max}/\Gamma^{\rm max}_{\uparrow\downarrow}$ vanishes or is very small at the end of the flow. Therefore, magnetic fluctuations are predominantly ferromagnetic at the end of the flow. On the other hand, $\Delta\Gamma_{\rm max}$ increases as $\mu_{\rm eff}$ approaches VHS: for both $U = 3t$ and $U = 4t$, $\Delta\Gamma_{\rm max}$ is the largest in the case $\bar{\mu} = 0.8t$.

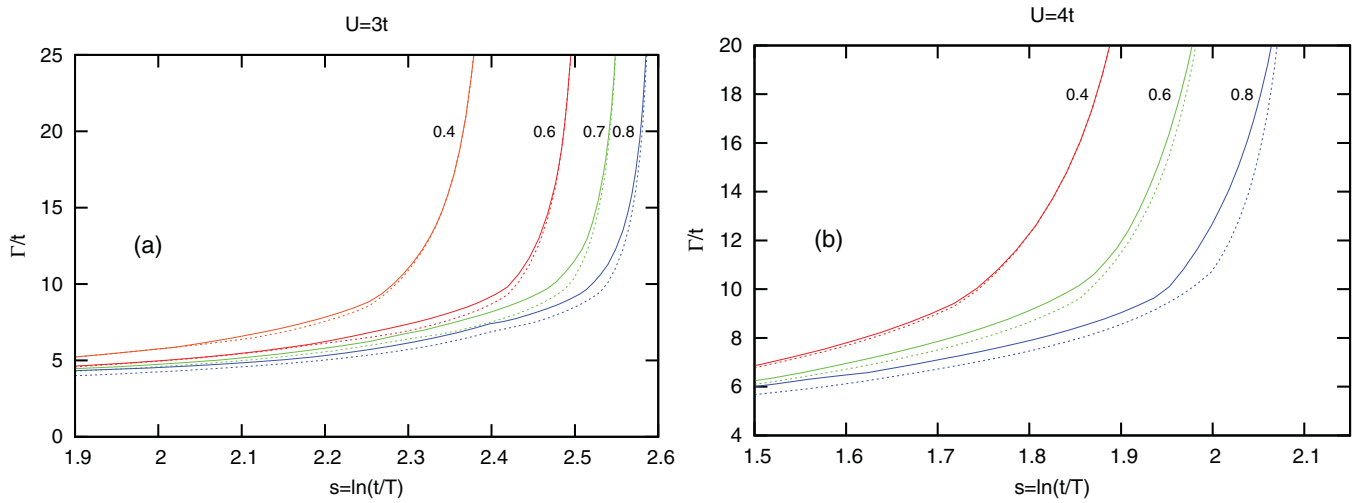

FIG. 5. (Color online) The scale profiles of $\Gamma^{\rm max}_{\uparrow\downarrow}$ (solid lines) and $\Gamma^{\rm max,E}_{\uparrow\downarrow}$ (dashed lines) (see text) in the case $h = 0$: (a) $U = 3t$, (b) $U = 4t$ for different choices of the chemical potential $\bar{\mu}$ (shown by numbers) yielding Fermi level below VHS ($\mu_{\rm eff} < 0$).

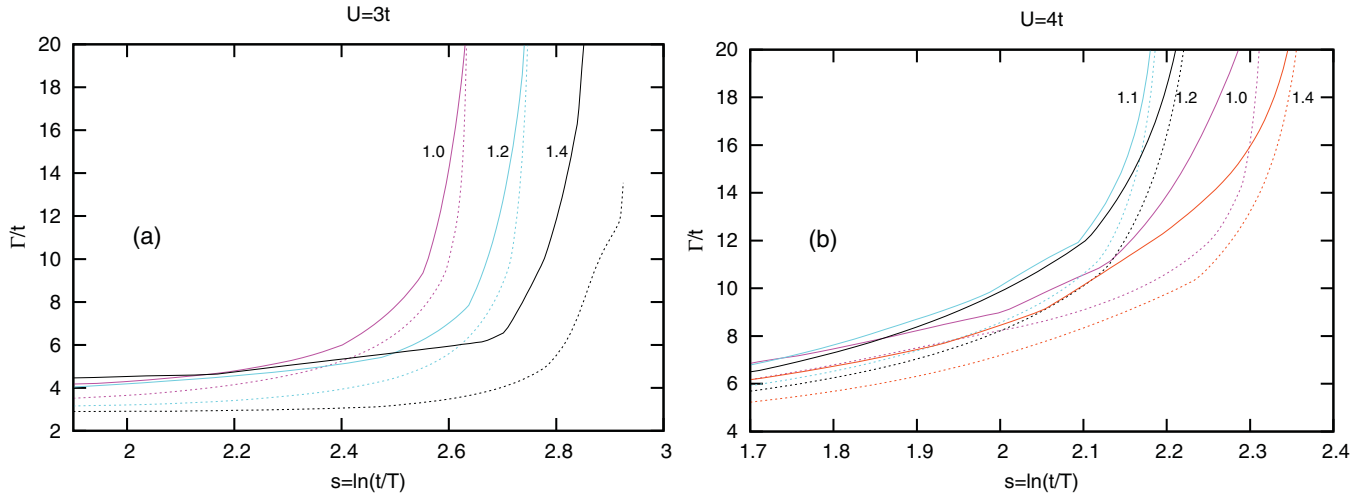

FIG. 6. (Color online) The same as in Fig. 5 for Fermi level being above VHS ($\mu_{\rm eff} > 0$).

This means that, in the vicinity of VHS, the ferromagnetic fluctuations hardly dominate over incommensurate ones.

For $\mu_{\rm eff} > 0$ (see Fig. 6), the difference $\Delta\Gamma_{\max}$ is nonzero up to the lowest temperatures where $\Gamma_{\max}$ diverges. Moreover, the ratio $\Delta\Gamma_{\max}/\Gamma^{\max}_{\uparrow\downarrow}$ increases as μ increases. We interpret this as that the incommensurate fluctuations are dominating over the ferromagnetic ones. In the case $\bar{\mu} = 1.0t$, where the temperature dependence of $\mu_{\rm eff}(s)$ is strongly nonmonotonous [see Fig. 3(b)], which is possibly related with invalidity of ansatz (16) and (21) in this regime, and causes the shift of the point of vertex diverging to substantially lower temperatures. This case should be considered more correctly in further elaborated studies.

In the next section, we introduce a small magnetic field to investigate magnetic properties of the system.

B. Magnetization in the finite magnetic field

In this section, we supplement the picture in the zero magnetic field considered above by the results for magnetic response in the finite magnetic field. In the case $h > 0$, we have $\mu_{\rm eff\uparrow} \neq \mu_{\rm eff\downarrow}$ due to spin dependence of the spectrum parameters $t_{{\rm eff},\sigma}, t'_{{\rm eff},\sigma}$, and Σ_σ and, to a small extent, due to the presence of magnetic field. At low scales (high temperatures), the spectrum parameters do not depend on the spin projection substantially and $\mu_{\rm eff\uparrow} - \mu_{\rm eff\downarrow} \approx 2h$, but with increasing the scale (lowering temperature), the strong spin dependence can be realized, which is a manifestation of exchange enhancement.

The strength of magnetic response is characterized by the magnetization m, which can be easily calculated using current parameters of the electronic spectrum $\delta t_\sigma, \delta t'_\sigma, \Sigma_\sigma$ (we remind that the frequency dependence of the self-energy is neglected):

$$m = \frac{1}{2N}\sum_{\mathbf{k}}(f_{\mathbf{k}\uparrow} - f_{\mathbf{k}\downarrow}). \tag{23}$$

Figure 7 shows the comparison of the scale profiles of magnetization m for different bare chemical potentials. For $\mu_{\rm eff}$ above VHS, we find slightly negative m at the end of the flow for both the cases $U = 3t$ and $U = 4t$. This is possibly related to an influence of incommensurate magnetic fluctuations above VHS, as conjectured from the results in zero magnetic field. Below VHS, where dominating ferromagnetic fluctuations were observed in the absence of magnetic field, the magnetic response to magnetic field becomes positive and considerable, especially in the vicinity of VHS: the maximal value of m at the end of the flow increases, but the temperature of sharp increase of the magnetization becomes lower as μ increases. Note that the absolute values of magnetization are rather small ($m \ll 2n$) at the end of the flow. To verify the fulfillment of the Mermin-Wagner theorem, we fit the data for magnetization taken at lowest temperatures of the flow to $m \propto h^\alpha$ dependence (see Fig. 8), which gives $\alpha \in (0.46, 0.83)$ depending on the chemical potential μ. In the vicinity of VHS level ($\bar{\mu} = 1.0t, 1.1t$) for $U = 4t$, the magnetization is somewhat larger at the end of the flow, in particular, $\alpha = 0.17$ at $\bar{\mu} = 1.1t$. Additionally, in this case, magnetization tends to saturate at lowest temperatures with increasing the magnetic field (not shown). For these chemical potentials, the renormalized Fermi level lies very near VHS and the Mermin-Wagner theorem may not be fulfilled to a good accuracy. On the other hand, these cases are on the borderline between the regions of strong ferromagnetic and incommensurate fluctuations.

The temperature dependence of the exponent α is of particular interest, since it allows us to investigate the magnetic properties of the system while entering the region of strong magnetic fluctuations. It is obvious that at high temperatures $m \propto h$ ($\alpha = 1$), but at low temperatures this relation can be violated due to fluctuations. To determine the temperature of the crossover into the regime with strong ferromagnetic fluctuations, we adopt the criterion $\alpha = 1/3$, dictated by the mean-field value of the critical exponent at the conventional magnetic phase transition. We denote the crossover scale as s^* [the corresponding temperature is $T^* = t\exp(-s^*)$].

Figure 9 shows the comparative (with respect to the magnetic field) representation of m/h and $m/h^{1/3}$ scale profiles for different positions of Fermi level below VHS in the case $U = 4t$. In the cases $\bar{\mu} = 0.4t$ and $0.6t$, the

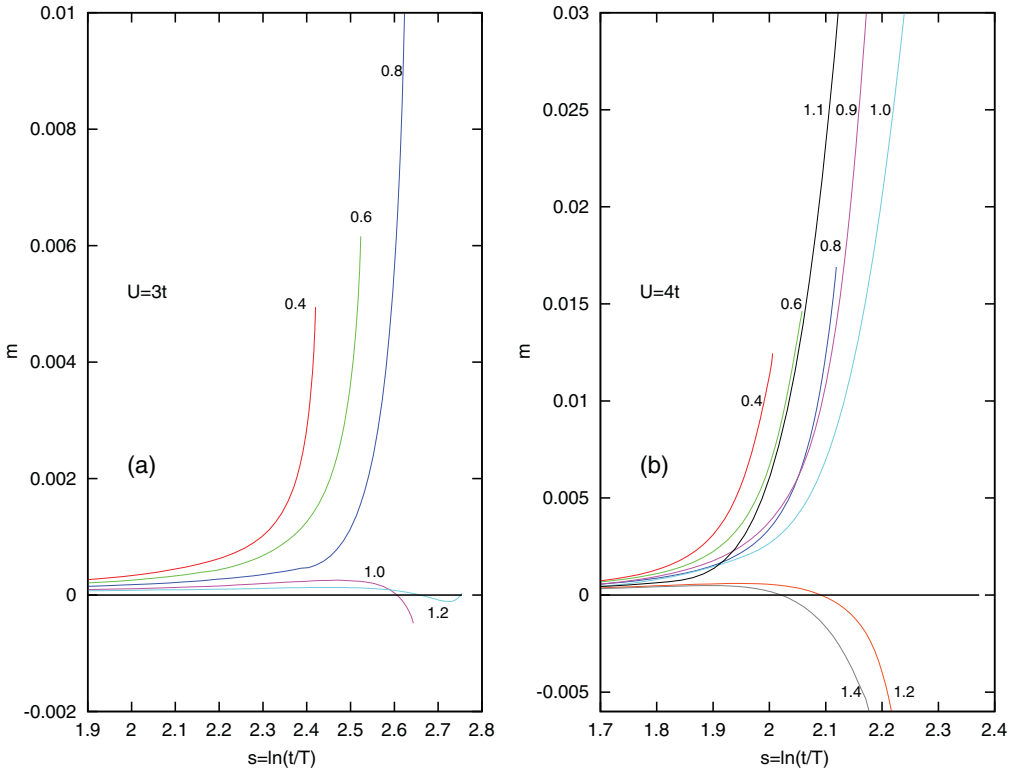

FIG. 7. (Color online) The magnetization scale profiles in the field $h = 10^{-4}t$ for different chemical potential $\bar{\mu}$ specified by numbers: (a) $U = 3t$, (b) $U = 4t$.

crossover scale is reached within the flow and lies near its end, while in the case $\bar{\mu} = 0.9t$, it is beyond the flow and is obtained by an extrapolation. Therefore, increasing $\bar{\mu}$ tends to decrease T^*. We do not find a well-resolved crossover scale at $U = 3t$, but we note that the system is close to it at the end of the flow in the case $\bar{\mu} = 0.4t$, where the magnetic fluctuations tend to be commensurate. This means that, at $U = 3t$, crossover to ferromagnetic ordering can be realized only at extremely low temperatures, which are not available within the present approach. For the case $\mu_{\text{eff}} > 0$ and both $U = 3t$ and $U = 4t$, we find a relatively weak response, which becomes negative close to the end of the flow, as discussed above.

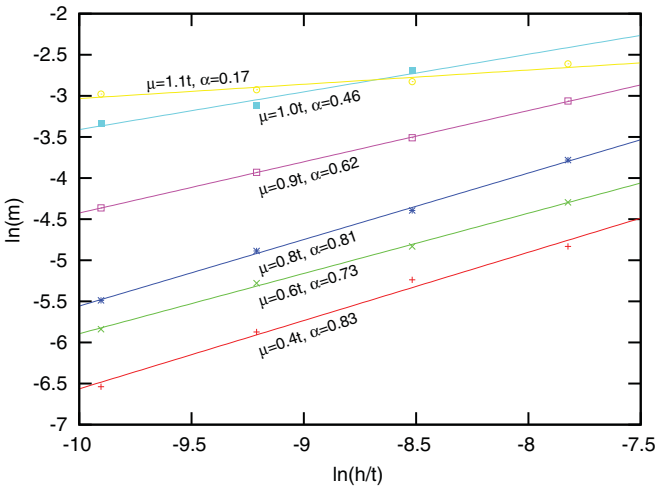

FIG. 8. (Color online) The logarithmic plots of the dependence $m(h)$ and its fit to $m \propto h^{\alpha}$. The chemical potentials $\bar{\mu}$ and fitted α are shown near the plots.

The distribution of temperatures T_{min} and T^* for different chemical potentials yields a natural connection between zero-field (T_{min}) and finite-field (T^*) results. We find that both T_{min} and T^* decrease as the system approaches VHS, which is possibly an effect of incommensurate magnetic fluctuations and temperature smearing of VHS (above van Hove filling, the DOS falls down faster than below it); below VHS, we obtain $T^* < T_{\text{min}}$. However, in the case $\bar{\mu} = 1.1t$, we find $T^* > T_{\text{min}}$, which is possibly connected to the above-discussed violation of the Mermin-Wagner theorem in a close vicinity above VHS.

C. Phase diagram

In this section, we summarize the results obtained in zero (Sec. IV A) and finite (IV B) magnetic fields and compare our results with the results of previous approaches. The phase diagram constructed in terms of renormalized Fermi level μ_{eff} (see discussion in Sec. IV A) and Coulomb interaction U is shown in Fig. 10.

In the case $\mu_{\text{eff}} < 0$, the large region on the phase diagram is found where magnetic fluctuations are predominantly commensurate. In small finite magnetic fields at $U = 3t$, a crossover from paramagnetic to ferromagnetic order is observed well beyond the flow, while at $U = 4t$, the crossover to ferromagnetic state is well resolved in the close vicinity

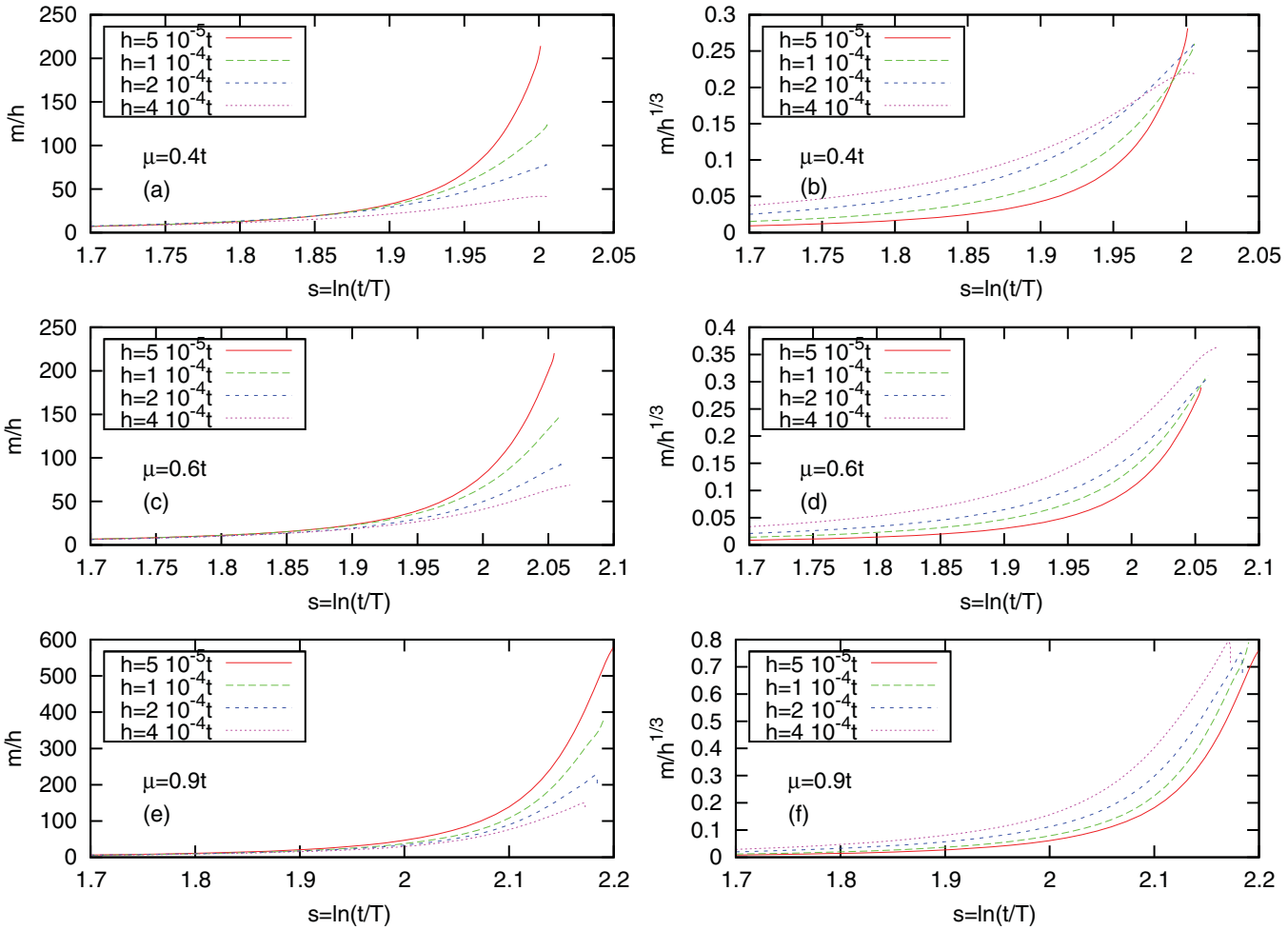

FIG. 9. (Color online) The scale profiles of ratios m/h [(a), (c), and (e)] and $m/h^{1/3}$ [(b), (d), and (f)] for $U = 4t$ at different small magnetic fields: $h/t = (5,10,20,40) \times 10^{-5}$ and different bare chemical potentials $\bar{\mu}$, the values of which are shown explicitly.

of the end of the flow. In the case $\mu_{\text{eff}} > 0$ (excluding the region of near vicinity of Fermi level to VHS), we do not find commensurate magnetic fluctuations to be dominating; they are completely replaced by incommensurate fluctuations with corresponding maximal vertex $\Gamma^{\max}_{\uparrow\downarrow}$ being diverging in the zero magnetic field. This conclusion agrees with the result in the finite magnetic field, where the magnetization m becomes slightly negative at low temperatures. Therefore, we conclude that ferromagnetic order is suppressed by incommensurate magnetic fluctuations if the Fermi level is above VHS. The case of μ_{eff} very near but above VHS is worthy of special attention: In the case $U = 3t$, we find incommensurate magnetic fluctuations in the zero magnetic field and no indication of ferromagnetic ordering in the finite field. However, very near VHS at $U = 4t$, we find almost commensurate magnetic fluctuations in the zero magnetic field and ferromagneticlike behavior in the finite magnetic field. At the same time, in this case μ_{eff} depends nonmonotonously on μ and the magnetization on the value of the magnetic field. These states are shown by the "?" symbol in Fig. 10.

The mean-field and quasistatic approximation (MFA and QSA) boundary lines calculated in Refs. 20 and 21 are shown on the phase diagram in Fig. 10 for comparison [the effective chemical potential in MFA $\mu^{\text{MF}}_{\text{eff}} = \mu - Un/2$, and in QSA it is determined from the condition for electronic density $n(\mu_{\text{eff}}) = n_0(\mu)$, where $n_0(\mu)$ is the number of particles in the noninteracting model]. The critical interaction for stability of ferromagnetism within the present approach $U_c > 3t$ is somewhat larger then the QSA and the mean-field resuts $[U_c(\mu_{\text{eff}} = 0) \approx 2t]$, which naturally suggests that the account for the electronic correlations results in an enhancement of U_c.

The results of this paper partly agree with those calculated within fRG approach without self-energy effects[29,39] ($\Sigma = 0$ fRG approach, see Fig. 10), obtained by studying the temperature dependences of magnetic and superconducting susceptibilities in zero magnetic field. The lower threshold for ferromagnetism U_c obtained in this paper appears to be finite, contrary to $\Sigma = 0$ fRG. At the same time, away from VHS, these two approaches qualitatively agree.

The comparison of different approaches MFA, QSA, $\Sigma = 0$ fRG, and SE fRG shows a step-by-step restriction of the size of the ferromagnetic region. Ferromagnetism is practically absent for $\mu_{\text{eff}} > 0$ within SE fRG, but not restricted with respect to previous approaches in the case $\mu_{\text{eff}} < 0$. Above VHS, ferromagnetism is destroyed by well-resolved incommensurate magnetic fluctuations, while below VHS, quantum commensurate fluctuations dominate.

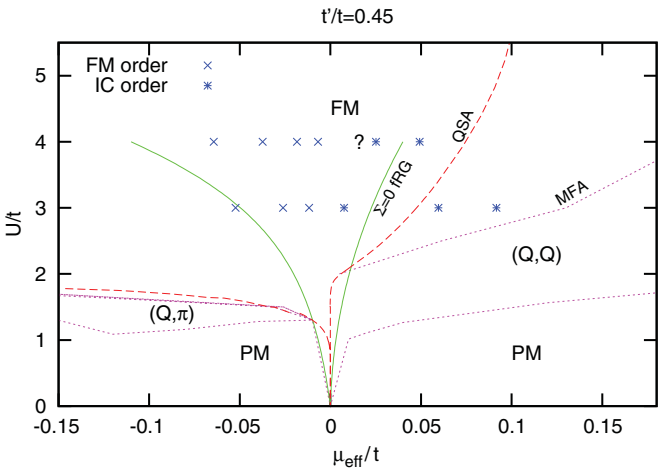

FIG. 10. (Color online) Summary magnetic phase diagram in the vicinity of VH filling in $\mu_{\text{eff}} - U$ plane, $t' = 0.45t$, obtained within the mean-field (Ref. 20) (short-dashed lines, $\mu_{\text{eff}}^{\text{MF}} = \mu - Un/2$, where n is the electronic density), $\Sigma = 0$ fRG (Ref. 29) (solid lines), QSA (Ref. 21) (long-dashed lines), and present SE fRG (symbols) approaches (see text). The boundary lines corresponding to $\Sigma = 0$ fRG and QSA approaches separate ferromagnetic and paramagnetic regions below van Hove filling and ferromagnetic and incommensurate magnetic phases above van Hove filling.

V. CONCLUSIONS

In this paper, we present a fRG treatment of magnetic order in the Hubbard model, controlled by the Fermi level being in the vicinity of van Hove singularity (VHS) and on-site Coulomb interaction. The introduced version of fRG accounts for self-energy corrections, which implies a proper account of the Fermi surface moving as the temperature decreases. The following aspects of this problem are investigated: the renormalization of vertices in the zero magnetic field, spin splitting in the finite field, finite-temperature behavior, and the electronic spectrum renormalization. Correlation effects do not change substantially the form of the electronic spectrum, which is characterized by t'/t. However, the renormalized ratio t'/t monotonously increases as the Fermi level rises toward VHS.

We find that magnetic properties of the system are substantially asymmetric with respect to the Fermi level position relative to VHS. In particular, ferromagnetic ordering is strongly suppressed above VHS due to competition with incommensurate magnetic fluctuations. Below VHS, we find precursors of ferromagnetic ordering at low temperatures and not too small interaction (of order of half-bandwidth). The temperature of the crossover to the regime of strong ferromagnetic fluctuations decreases as the Fermi level elevates toward VHS.

The asymmetry is connected with the electronic topological transition, which occurs when the Fermi level crosses VHS. At this transition, the curvature of the Fermi surface changes its sign, being singular at VHS points of the Brillouin zone. At $\mu_{\text{eff}} > 0$, the flat parts of the Fermi surface appear in the vicinity of VHS points ("quasinesting" situation), which results in enhancement of the incommensurate fluctuations.

The results of the present approach improve the results of the mean-field approximation[20] and quasistatic approach[21] and agree with previous fRG study[29] for the position of the Fermi level away from VHS. The Mermin-Wagner theorem is also shown to be fulfilled to a good accuracy in the present approach in the most part of the phase diagram. The magnetic field dependence of magnetization demonstrates power-law behavior with the exponents $\alpha \in (0.62, 0.83)$.

For the Fermi level above VHS the ferromagnetic phase is practically absent. This explains qualitatively the magnetic behavior of lanthanum-doped one-layer ruthenates $Sr_{2-x}La_xRuO_4$. The parameters of the d_{xy} band of Sr_2RuO_4 are $t'/t = -0.405$ and $n \sim 4/3$. The particle-hole transformation $c_{i\sigma} \to (-1)^i c_{i\sigma}^\dagger$ results in the replacements $t' \to -t'$, $n \to 2 - n$. Therefore, in terms of new variables, we have $t'/t = 0.405$ and $n \sim 2/3$, which implies $\mu_{\text{eff}} \simeq 0.1t$. In this case, we expect spiral magnetic ordering in the ground state for $U \sim 3t$.

Doping Sr_2RuO_4 by lanthanum corresponds to the decrease of electronic filling n and the approach of the Fermi level to the VHS of the γ band. This, however, results in strong enhancement of the magnetic susceptibility, and not in the transition into the ferromagnetic state, which agrees with the experimental data.[8] The non-Fermi-liquid behavior of doped by lanthanum Sr_2RuO_4 (Ref. 8) can be possibly related to the nonmonotonous temperature dependence of the Fermi level near VHS in the present approach, which neglects nonquasiparticle contributions. These contributions may therefore be important for the Fermi level near VHS (see, e.g. Ref. 38), which is the subject of future study.

Enhancement of susceptibility observed in the $Ca_{2-x}Sr_xRuO_4$ compound at $x = 0.5$ corresponds to the position of the Fermi level between VHS and the γ-band edge. This agrees qualitatively with our conclusion that the position of the Fermi level below VHS favors strong ferromagnetic fluctuations. A similar picture can be seemingly applied to the bilayer compound $(Sr_{1-x}Ca_x)_3Ru_2O_7$.[17]

The results obtained demonstrate an important role of many-electron renormalizations of the electron spectrum, in particular, of the chemical potential, in the presence of VHS. This fact can be crucial for the criteria and properties of weak itinerant ferromagnetism. Another important point is that peculiarities of ferromagnetic ordering related to the presence of VHS can not be even qualitatively captured by any elaborate method based on DOS consideration only.

The obtained finite-temperature picture, in particular, the relation of the character of magnetic fluctuations to the position of the Fermi level and absence of the long-range order (which is stated by the Mermin-Wagner theorem), should be supplemented by a zero-temperature study of this problem. Investigation of the effect of finite (but not too small) magnetic field and possibility of the metamagnetic transitions is also of interest. Another unsolved problem is a unified description of weak and strong ferromagnets, which can receive new insights from weak-coupling investigations of the Hubbard model.

ACKNOWLEDGMENTS

We are grateful to W. Metzner, H. Yamase, and M. Salmhofer for stimulating discussions. This work was supported in part by the Partnership Program of the

Max-Planck Society, the project Quantum Physics of Condensed Matter of the Presidium of Russian Academy of Science, President Program of Scientific Schools Support 4711.2010.2, "Dynasty" foundation, projects of RFBR No. 11-02-00931-a, No. 11-02-00937-a, and project of young scientists of Ural Branch of RAS M–8.

APPENDIX: PROJECTING POINTS

To parametrize the momentum dependence of the self-energy and vertex, we introduce a set of points in the Brillouin zone (below we refer to them as projecting points, PPs), so that the values of functions at these points represent the function. In previous studies,[28] this set of the points was chosen as an intersection of lines of constant angles (located at the center of patches) with FS, which was assumed to be fixed. Since we account for momentum dependence of the self-energy and vertex more accurately, we supplement this set of PPs at FS by a corresponding set in the vicinity of FS by choosing additional points belonging to shifted FS and call it an auxiliary set of PPs. However, since moving of FS is a continuous process, we apply the discrete Runge-Kutt procedure (RKP) to solve the system of differential equations numerically, which causes some complications in the definition of PP.

At any discrete step of RKP, we introduce the PPs of the following types: (i) main PPs, which belong to FS, determined by the chemical potential μ, and the self-energy $\Sigma_{\mathbf{k}\sigma}$ at the beginning of the step; (ii) auxiliary PPs, which are determined analogously to main PPs, with μ being shifted by $\delta\mu_\sigma$ for different spin projections, and $\delta\mu_\sigma$ is determined by typical shift of momentum-independent part of self–energy Σ_σ at previous step; (iii) current PPs, which are determined by current $\Sigma_{\mathbf{k}\sigma}$ within the step. Note that, at the beginning of the step, the main PPs coincide with current ones. Introduction of the auxiliary PPs set is needed since, due to definition of the main PPs set, the functions chosen to represent momentum dependence of Σ $(\cos k_x + \cos k_y, \cos k_x \cos k_y, 1)$ are linearly dependent at the constant energy set (see Sec. III B), which does not allow us to use them for linear regression of Σ derivatives. Therefore, an additional set of PPs is needed; the calculation of the vertex near current FS allows us to expand the vertex linearly beyond simple projecting ansatz (see detail explanation in Sec. III C), which was used in earlier studies.

RKP makes its step using the vertex and self-energy derivatives calculated at the intermediate (current) value of argument s at fixed (during the step) sets of main and auxiliary PPs. From this, we extract derivatives $\dot{\delta}t_\sigma$, $\dot{\delta}t'_\sigma$, and $\dot{\Sigma}_\sigma$ (see Sec. III B). However, the right-hand side of fRG equations contains the *current* self-energy function and vertex function, projected on the current FS. RKP allows us to calculate this current self-energy function and use it to determine the current FS and corresponding current PPs set. Then, we apply the procedure of Sec. III C, accounting for the influence of the FS moving on the current value of the projected vertex.

[1] M. Matsuda, M. Fujita, K. Yamada, R. J. Birgeneau, Y. Endoh, and G. Shirane, Phys. Rev. B **65**, 134515 (2002); M. Fujita, K. Yamada, H. Hiraka, P. M. Gehring, S. H. Lee, S. Wakimoto, and G. Shirane, *ibid.* **65**, 064505 (2002).

[2] D. Haug, V. Hinkov, A. Suchaneck, D. S. Inosov, N. B. Christensen, Ch. Niedermayer, P. Bourges, Y. Sidis, J. T. Park, A. Ivanov, C. T. Lin, J. Mesot, and B. Keimer, Phys. Rev. Lett. **103**, 017001 (2009); A. Suchaneck, V. Hinkov, D. Haug, L. Schulz, C. Bernhard, A. Ivanov, K. Hradil, C. T. Lin, P. Bourges, B. Keimer, and Y. Sidis, *ibid.* **105**, 037207 (2010).

[3] M. Braden, Y. Sidis, P. Bourges, P. Pfeuty, J. Kulda, Z. Mao, and Y. Maeno, Phys. Rev. B **66**, 064522 (2002).

[4] A. P. Mackenzie and Y. Maeno, Rev. Mod. Phys. **75**, 657 (2003).

[5] M. Sigrist and K. Ueda, Rev. Mod. Phys. **63**, 239 (1991).

[6] I. I. Mazin and D. J. Singh, Phys. Rev. Lett. **79**, 733 (1997).

[7] K. M. Shen, N. Kikugawa, C. Bergemann, L. Balicas, F. Baumberger, W. Meevasana, N. J. C. Ingle, Y. Maeno, Z.-X. Shen, and A. P. Mackenzie, Phys. Rev. Lett. **99**, 187001 (2007).

[8] N. Kikugawa, C. Bergemann, A. P. Mackenzie, and Y. Maeno, Phys. Rev. B **70**, 134520 (2004).

[9] E. Ko, B. J. Kim, C. Kim, and H. J. Choi, Phys. Rev. Lett. **98**, 226401 (2007).

[10] S.-C. Wang *et al.*, Phys. Rev. Lett. **93**, 177007 (2004).

[11] S. Nakatsuji, D. Hall, L. Balicas, Z. Fisk, K. Sugahara, M. Yoshioka, and Y. Maeno, Phys. Rev. Lett. **90**, 137202 (2003).

[12] P. Steffens, O. Friedt, Y. Sidis, P. Link, J. Kulda, K. Schmalzl, S. Nakatsuji, and M. Braden, Phys. Rev. B **83**, 054429 (2011).

[13] L. Capogna, E. M. Forgan, S. M. Hayden, A. Wildes, J. A. Duffy, A. P. Mackenzie, R. S. Perry, S. Ikeda, Y. Maeno, and S. P. Brown, Phys. Rev. B **67**, 012504 (2003).

[14] S. A. Grigera *et al.*, Science **294**, 329 (2001); C. Pfleiderer, S. R. Julian, and G. G. Lonzarich, Nature (London) **414**, 427 (2001).

[15] B. Binz and M. Sigrist, Europhys. Lett. **65**, 816 (2004).

[16] H. Yamase and A. Katanin, J. Phys. Soc. Jpn. **76**, 073706 (2007); H. Yamase, Phys. Rev. B **76**, 155117 (2007).

[17] Z. Qu, L. Spinu, H. Yuan, V. Dobrosavljević, W. Bao, J. W. Lynn, M. Nicklas, J. Peng, T. Liu, D. Fobes, E. Flesch, and Z. Q. Mao, Phys. Rev. B **78**, 180407 (2008).

[18] D. R. Penn, Phys. Rev. **142**, 350 (1966).

[19] H. J. Schulz, Phys. Rev. Lett. **64**, 1445 (1990).

[20] P. A. Igoshev, M. A. Timirgazin, A. A. Katanin, A. K. Arzhnikov, and V. Yu. Irkhin, Phys. Rev. B **81**, 094407 (2010).

[21] P. A. Igoshev, A. A. Katanin, and V. Yu. Irkhin, Sov. Phys. JETP **105**, 1043 (2007) [ZhETF **132**, 1187 (2007)]; P. A. Igoshev, A. A. Katanin, H. Yamase, and V. Yu. Irkhin, J. Magn. Magn. Mater. **321**, 899 (2009).

[22] T. Okabe, Phys. Rev. B **57**, 403 (1998).

[23] R. Hlubina, S. Sorella, and F. Guinea, Phys. Rev. Lett. **78**, 1343 (1997); R. Hlubina, Phys. Rev. B **59**, 9600 (1999).

[24] A. A. Katanin, A. P. Kampf, and V. Yu. Irkhin, Phys. Rev. B **71**, 085105 (2005).

[25] M. Salmhofer and C. Honerkamp, Prog. Theor. Phys. **105**, 1 (2001).

[26] D. Zanchi and H. J. Schulz, Phys. Rev. B **61**, 13609 (2000).

[27] C. J. Halboth and W. Metzner, Phys. Rev. B **61**, 7364 (2000).

[28] C. Honerkamp and M. Salmhofer, Phys. Rev. B **64**, 184516 (2001).

[29] A. A. Katanin and A. P. Kampf, Phys. Rev. B **68**, 195101 (2003).

[30] A. Katanin, Phys. Rev. B **81**, 165118 (2010).

[31] C. Honerkamp, D. Rohe, S. Andergassen, and T. Enss, Phys. Rev. B **70**, 235115 (2004).
[32] W. Metzner, J. Reiss, and D. Rohe, Phys. Status Solidi B **243**, 46 (2005).
[33] M. Salmhofer, C. Honerkamp, W. Metzner, and O. Lauscher, Prog. Theor. Phys. **112**, 943 (2004); R. Gersch, C. Honerkamp, D. Rohe, and W. Metzner, Eur. Phys. J. B **48**, 349 (2005); R. Gersch, J. Reiss, and C. Honerkamp, New J. Phys. **8**, 320 (2006); R. Gersch, C. Honerkamp, and W. Metzner, *ibid*. **10**, 045003 (2008).
[34] M. Salmhofer, Ann. Phys. (NY) **16**, 171 (2007).
[35] T. Moriya, J. Phys. Soc. Jpn. **40**, 933 (1976); *Spin Fluctuations in Itinerant Electron Magnetism* (Springer, Berlin, 1985).
[36] A. A. Katanin, Phys. Rev. B **70**, 115109 (2004).
[37] Without introducing approximations, the final results should not depend on the choice of $\mu(T)$ dependence provided that the final renormalized chemical potential or particle number is fixed.
[38] V. Yu. Irkhin, A. A. Katanin, and M. I. Katsnelson, Phys. Rev. Lett. **89**, 076401 (2002).
[39] A. A. Katanin, H. Yamase, and V. Yu. Irkhin, J. Phys. Soc. Jpn. **80**, 063702 (2011).